HHS Public Access

Author manuscript

Biochem Biophys Res Commun. Author manuscript; available in PMC 2020 October 29.

Published in final edited form as:

Biochem Biophys Res Commun. 2019 October 29; 519(1): 61–66. doi:10.1016/j.bbrc.2019.08.126.

Potent antiviral HIV-1 protease inhibitor combats highly drug resistant mutant PR20

Daniel W. Kneller[†], **Johnson Agniswamy**[†], **Arun K. Ghosh**[‡], **Irene T. Weber**[*,†,§]

[†]Department of Biology, Georgia State University, Atlanta, GA, 30303, USA

[‡]Department of Chemistry and Department of Medicinal Chemistry, Purdue University, West Lafayette, IN, 47907, USA

[§]Department of Chemistry, Georgia State University, Atlanta, GA, 30303, USA

Abstract

Drug-resistance threatens effective treatment of HIV/AIDS. Clinical inhibitors, including darunavir (**1**), are ineffective for highly resistant protease mutant PR20, however, antiviral compound **2** derived from **1** with fused tricyclic group at P2, extended amino-benzothiazole P2' ligand and two fluorine atoms on P1 shows 16-fold better inhibition of PR20 enzyme activity. Crystal structures of PR20 and wild-type PR complexes reveal how the extra groups of **2** counteract the expanded ligand-binding pocket, dynamic flaps, and faster dimer dissociation of PR20.

Keywords

Drug resistance; HIV protease; antiretroviral inhibitor; structure-based design; X-ray crystallography

1. Introduction

The HIV/AIDS pandemic comprises about 38 million infected individuals at present and almost 60% of them receive antiretroviral therapy [1] and showing decreased mortality [2]. This success is undermined by treatment failure due to drug resistance and persistent reservoirs of latent virus [3].

Antiviral HIV-1 protease (PR) inhibitors (PIs) are effective for therapy, and darunavir (DRV, **1**) (Figure 1) is approved for first line treatments[4,5]. Its favorable properties include picomolar affinity for PR, high genetic barrier to resistance[6,7], inhibition of precursor autoprocessing[8,9] and inhibition of PR dimerization[10]. Nevertheless, DRV-resistant viral strains pose a problem[11]. Resistance to PIs evolves primarily by mutations in PR. Mutations of >35 of the 99 residues in PR are associated with resistance to one or more PIs[12]. Highly-resistant PR variants in clinical isolates have different combinations of about

[*]Corresponding author: iweber@gsu.edu Phone: (+1) 404-413-5411.

Conflicts of interest

None declared.

20 mutations and diminish the effectiveness of PIs by a variety of molecular mechanisms[13–17].

An HIV-1 PR variant with 20 mutations derived from a clinical isolate (PR20) has been characterized and used as a prototype to assess investigational PIs[18,19]. Compared to wild-type PR, PR20 shows drastically reduced inhibition by clinical PIs with over 8,000-fold worse binding affinity for DRV[8]. Moreover, autoprocessing of its precursor is unaffected by **1** unlike the wild-type precursor[8]. Structures of PR20 reveal an expanded ligand-binding cavity, which contributes to decreased affinity for PIs[18] and fewer interactions with substrate analogs. Crystallography and NMR spectroscopy experiments suggest a PI-independent mechanism for poor PI affinity due to increased mobility of the two flexible flap regions[18,20–22]. Finally, PR20 has a higher rate of dimer dissociation than wild-type enzyme, which further weakens drug binding[23]. PR20 contains four mutations in the ligand binding site (D30N, V32I, I47V, I84V) which act in the S1/S1′ and S2/S2′ pockets to decrease hydrophobic interactions with inhibitors[18,24]. The dimer structure of PR20/**1** and key mutations are shown in Figure 1B. PR20 provides an excellent prototype to assess the effectiveness of new inhibitors designed to combat highly resistant variants[24,25].

Potent new PIs are urgently required to target resistant variants such as PR20, but must also feature improved genetic barrier to resistance and better CNS penetration[26] for effective treatment. Recently, antiviral compound GRL-142 (**2**) was reported to show picomolar inhibition of PR activity, high barrier to resistance, and improved penetration of the blood-brain barrier compared to **1**[27,28]. Compound **2** was designed with modifications of three moieties of DRV (Figure 1A) to target drug-resistant variants[29]: P2 *bis*-tetrahydropyranofuran (*bis*-THF) is replaced by a “crown-like” *Cm*-THF; P2′-aniline is substituted by a cyclopropyl-amino-benzothiazole (Cp-Abt) group, and two fluorine atoms modify the P1-phenyl group to create *bis*-fluoro-benzyl (*bis*-FBz). Fluorination of PIs has been shown to introduce halogen-bonds with protease[25,30] and increase lipophilicity[31,32].

Here we report that **2** is an order of magnitude better than **1** in inhibiting enzyme activity of drug-resistant PR20. The crystal structure of PR20/**2** complex reveals how the inhibitor effectively fills the expanded ligand binding site and stabilizes the dynamic flaps and dimer interface.

2. Materials and Methods

2.1. PR20 expression and purification

A synthetic 99 amino acid gene derived from the clinical isolate for PR20[19] was expressed in E. coli, purified, and folded as described in [18].

2.2. Kinetic inhibition assay

Compound **2** (>95% purity by HPLC), developed in Ghosh Laboratory at Purdue University, was dissolved in 100% DMSO. The kinetic inhibition value (K_i) of **2** for PR20 was measured using a FRET-substrate (BACHEM H-2992) at 37°C and pH 5.6 based spectroscopic assay as described in [33].

2.3 X-ray crystallography

PR20 at 4 mg/mL was mixed with **2** at 1:5 molar ratio. Crystals were grown using hanging-drop vapor diffusion in 1.8 M sodium chloride, 0.1 M sodium acetate pH 5.5, 0.1 M yttrium chloride, and cryo-protected in mother liquor containing 30% glycerol prior to freezing with liquid nitrogen. Diffraction data were collected on the SER-CAT 22ID beamline at the Advanced Photon Source, Argonne National Laboratory (Argonne, IL). X-ray data were processed and scaled using HKL-2000[34] before solving the structure by molecular replacement in phaser[35] from CCP4[36] with PR20/GRL-5010A (4YHQ)[25] as initial model. The structure was refined using COOT[37] and REFMAC5[38] applying anisotropic B-factors. Hydrogen bonds (2.4–3.5 Å) and hydrophobic contacts (3.6–4.2 Å) were inferred from interatomic distances and chemistry. Figures were generated using PyMOL[39]. Coordinates and structure factors for PR20/**2** have been deposited in the Protein Data Bank with accession code 6PRF.

3. Results

3.1. Compound 2 is more effective than DRV for PR20

Investigative compound **2** has an enzyme inhibition constant (K_i) of 14 pM for wild-type PR[27], comparable to the value of 5–10 pM for the best clinical inhibitor, DRV[40,41]. **2** exhibits a K_i of 2.5 ± 0.5 nM for PR20, approximately 1200-fold worse than for PR. However, this K_i for PR20 is 16-fold better than the 40 nM value observed for DRV[8].

3.2. Overall structure of PR20/2

The crystal structure of the PR20 complex with **2** was refined to a R-factor of 15.2% at 1.21 Å resolution, the highest resolution to date for PR20 (Table 1). The asymmetric unit has a homodimer of PR20 (residues 1–99 and 1′−99′). Inhibitor **2** binds in the active site in two orientations with 0.5/0.5 relative occupancy related by ~180° rotation. An Fo-Fc omit map for one conformation of **2** is shown in Figure 2A. Residues 45–47, 50–51, 44′−48′, and 50′−52′ in the flap region, Asn30/30′ and Arg8/8′ also show two alternate conformations, each associated with one inhibitor orientation. The two alternate conformations show no significant differences in PR20 interactions with **2**. Inhibitor-binding interactions in PR20/**2** were compared with those in PR/**2** and PR20/**1** complexes.

3.3. Mutant PR20/2 compared to wild-type PR/2

The PR20/**2** structure was compared to two reported structures of wild-type PR/**2**. The equivalent 198 Cα atoms of the two PR/**2** (6BZ2, 5TYS) dimers[27,28] superpose onto PR20/**2** with Root mean square deviations (RMSDs) of 0.63 and 0.68 Å, respectively. The two PR/**2** dimers are nearly identical (RMSD = 0.48 Å) with two conformations for **2** of almost equal occupancies. For clarity, the following analysis will describe significant differences in one **2** conformation in comparison to the major occupancy conformation of the higher resolution PR/**2** (6BZ2 at 1.67 Å) structure.

Polar interactions between PR20 and **2** are shown in Figure 2B. The wild-type PR/**2** complex has almost identical hydrogen bond and halogen interactions except for interactions

with the mutated residue D30N. Polar and non-polar interactions are described separately for P2 and P2' groups.

The bulky P2-*Crn*-THF on **2** binds in the S2 pocket (Fig 3A), where the two oxygen atoms form three hydrogen bonds with main-chain amides of residues 29 and 30 in both PR and PR20. The D30N mutation in PR20 substitutes a carboxylic acid for a carboxamide side-chain which enables formation of a 3.5 Å hydrogen bond with **2** which cannot occur for Asp30 in the PR structures. The P2-*Crn*-THF packs into the hydrophobic pocket of the S2 site forming 3 van der Waals contacts with Ile47 in PR. The S2 pocket of PR20 contains the drug-resistance mutations I47V and V32I. Mutation I47V produces one less hydrophobic contact, while the longer isoleucine side-chain in V32I introduces 3 new van der Waals contacts with **2** that are absent in PR. This observation is consistent with molecular dynamics simulations showing improved van der Waals interactions between a V32I single mutant and **2**[28]. Therefore, the three drug-resistance mutations in the S2 pocket of PR20 result in a net increase of one hydrogen bond and 2 hydrophobic interactions with the P2 group of **2** in comparison to those in the wild-type complex PR/**2**.

In the other protease subunit, the P2′-Cp-Abt group of **2** binds in the S2′ pocket (Fig 3B). In the PR/**2** structure, the side-chain carboxylate of Asp30′ forms a bifurcated hydrogen bond with the two nitrogen atoms of Cp-Abt. In PR20, the side-chain of the mutated D30′N is flipped 180° relative to its conformation in the other subunit. This orientation of Asn30′ forms a hydrogen bond with the P2′ amine of **2**, while also forming a hydrogen bond with the aspartate side-chain of N88′D in PR20. The B-value for Asn30′ side-chain in PR20/**2** is approximately half that of Asp30′ in PR/**2** and PR20/**1** (16 vs 33 and 28 $Å^2$), suggesting a more stable conformation. The main-chain of Val47′ in the PR20 flap is shifted by 0.5 Å relative to its position in PR, eliminating a hydrophobic interaction with the thiazole sulfur of **2**. However, the cyclopropyl moiety on **2** is shifted 1.5 Å towards the I47′V mutation, which introduces two hydrophobic contacts. Like in the S2 pocket, the larger V32′I mutation introduces a hydrophobic contact with **2**. Thus, PR20 shows favorable polar and hydrophobic interactions with the P2′ group of **2** despite multiple resistance mutations in the S2′ pocket.

In addition to the changes in the S2 and S2' pockets of PR20, the shorter side-chain of I84V mutation in the S1/S1′ pockets accounts for a net loss of 4 hydrophobic contacts with **2** compared to those in the wild-type complex. These altered interactions due to mutations in the active site of PR20 are expected to enhance affinity for inhibitor **2**.

3.4. Comparison of PR20 interactions with inhibitors 1 and 2

The crystal structure of PR20/**2** was compared to PR20/**1** (PDB: 3UCB) to understand the difference of inhibitory values. The bulky P2 *Crn*-THF of **2** forms 5 hydrophobic contacts with mutations I47V and V32I that cannot occur for *bis*-THF of **1** in the PR20/**1** structure, although the hydrogen bonds are conserved (Figure 4A). The P2′-Cp-Abt group on **2** is also larger than the P2′-aniline of **1**. Both inhibitors show similar interactions with I47′V and V32′I side-chains, however, the extended P2′ group of **2** introduces 10 more hydrophobic contacts with the side-chains of Asp29′ and Asn30′ (Figure 4B). The thiazole ring of **2**

forms a hydrogen bond with the Asn30′ amide, while the aniline amide of **1** interacts with the Asn30′ carbonyl. Moreover, the P2′ amine in **2** introduces a direct hydrogen bond with Asn30′ side-chain replacing a less favorable indirect water-mediated interaction in **1** (Figure 4C).

Difluorination of the P1-group of **2** enhances its penetration of the cell membrane and introduces halogen bonds with wild-type PR[28]. The P1 *bis*-FBz forms fluorine bonds with the Arg8′ side-chain and the main-chain amide of Ile50 at the flap tip. These halogen bonds bridge the S1 pocket and the dimer interface (Figure 4D). Arg8/8′ forms a critical intersubunit ion-pair with Asp29′/29 in most PR dimers[42]. In PR20/**1**, the larger side-chain of L10F mutation induces rotation of the side-chains of Arg8 and Arg8′, thus eliminating the ion-pair with Asp29′/29, which has been proposed to increase dissociation of PR20 dimers[18]. This rotated conformation of Arg8 and loss of its intersubunit ion-pair is observed in the S1′ pocket of both PR20/**1** and PR20/**2** structures where the identical P1′-isobutyl group is ~6 Å away from Arg8 (Figure 4E). However, in the S1 pocket of PR20/**2**, the fluorine bond between **2** and Arg8′ acts to overcome the effect of the L10′F mutation.

The P1 *bis*-FBz group of **2** introduces new hydrophobic contacts with PR20 that cannot occur for the smaller P1 of **1**. The fluorine atoms make additional contacts with residue Ile50 at the flap tip, which may decrease the mobility of the flaps and stabilize the binding of inhibitor **2** within the expanded active site cavity of PR20.

Overall, larger P2 and P2′ moieties for **2** relative to **1** introduce more van der Waals contacts with the expanded ligand binding pocket that contribute to better inhibition of PR20, although **2** is unable to make contacts with the shorter side-chain of I84V mutation. These observations in PR20 are consistent with molecular dynamic calculations comparing van der Waals interaction energies between **1** and **2** in PR[28]. Compared to DRV, compound **2** can form a larger number of direct polar interactions with PR20. A fluorine bond between the P1 of **2** and Arg8′ restores an inter-subunit ion-pair and may counteract the higher rate of dimer dissociation of PR20. The addition of a halogen bond bridge tethering one flap to the protease body stabilizes the dynamic flaps. These factors combine to deliver an order of magnitude better inhibition of compound **2** over DRV for PR20.

4. Discussion

Our studies of PR20 mutant address the key challenge of HIV drug resistance [8,24]. PR20 achieves decreased affinity for inhibitors by synergistic mechanisms of an expanded inhibitor-binding cavity, highly dynamic flaps, and accelerated dimer dissociation compared to wild-type enzyme. Clinical inhibitor **1**, the most potent for wild-type PR (5 pM), exhibits 8,000-fold worse binding affinity (40 nM) for PR20[8]. Compound **2** shows 16-fold better K_i than **1** for PR20 (2.5 nM). The larger *Crn*-THF at P2 and Cp-Abt at P2’ groups of **2** introduce additional hydrophobic and polar interactions with the mutated side-chains of the expanded ligand binding site. The fluorines of P1-*bis*-FBz of **2** create halogen bonds bridging the flap and Arg8′ to stabilize the dynamic flaps and restore an intersubunit ion-pair that may help to decrease the rate of dimer dissociation.

Compound **2** was developed using structure-guided drug design strategy for resistant PR. By incorporating larger P2/P2′ groups that fit into the expanded binding pocket and halogen flap interactions, **2** can inhibit PR20 better than the best current clinical PI. Future design may expand to modifications of the P1′ group. While these larger moieties of **2** help fill the expanded ligand binding pocket of PR20, other mutants exhibit few changes in the active site and diminish the potency of PIs through the effects of distal clusters of mutations[14]. In conclusion, antiviral inhibitor **2** is a noteworthy advance in the pursuit of potent inhibitors for resistant HIV.

Acknowledgments

We thank the staff at the Southeast Regional-Collaborative Access Team (SER-CAT) at the Advanced Photon Source, Argonne National Laboratory, for assistance during X-ray data collection. Supporting institutions may be found at http://www.ser-cat.org/members.html. Use of the Advanced Photon Source was supported by the U. S. Department of Energy, Office of Science, Office of Basic Energy Sciences, under Contract No. W-31-109-Eng-38.

Funding

This research was supported by the National Institute of Health grants AI150461 (ITW) and AI150466 (AKG) and a Georgia State University Molecular Basis of Disease fellowship.

References

[1]. UNAIDS, Global HIV & AIDS statistics - 2019 fact sheet | UNAIDS, (n.d.). https://www.unaids.org/en/resources/fact-sheet (accessed July 31, 2019).

[2]. WHO | Data and statistics, (2018). https://www.who.int/hiv/data/en/ (accessed January 25, 2019).

[3]. Phillips AN, Stover J, Cambiano V, Nakagawa F, Jordan MR, Pillay D, Doherty M, Revill P, Bertagnolio S, Impact of HIV Drug Resistance on HIV/AIDS-Associated Mortality, New Infections, and Antiretroviral Therapy Program Costs in Sub–Saharan Africa, J. Infect. Dis 215 (2017) 1362–1365. doi:10.1093/infdis/jix089. [PubMed: 28329236]

[4]. Koh Y, Nakata H, Maeda K, Ogata H, Bilcer G, Devasamudram T, Kincaid JF, Boross P, Wang Y-F, Tie Y, Volarath P, Gaddis L, Harrison RW, Weber IT, Ghosh AK, Mitsuya H, Novel bis-Tetrahydrofuranylurethane-Containing Nonpeptidic Protease Inhibitor (PI) UIC-94017 (TMC114) with Potent Activity against Multi-PI-Resistant Human Immunodeficiency Virus In Vitro, Antimicrob. Agents Chemother. 47 (2003) 3123–3129. doi:10.1128/AAC.47.10.3123-3129.2003.

[5]. Panel on Antiretroviral Guidelines for Adults and Adolescents, Guidelines for the Use of Antiretroviral Agents in Adults and Adolescents Living with HIV, (2016). https://aidsinfo.nih.gov/contentfiles/lvguidelines/adultandadolescentgl.pdf.

[6]. Lathouwers E, Wong EY, Luo D, Seyedkazemi S, De Meyer S, Brown K, HIV-1 resistance rarely observed in subjects using darunavir once-daily regimens across clinical studies, HIV Clin. Trials 18 (2017) 196–204. doi:10.1080/15284336.2017.1387690. [PubMed: 29143565]

[7]. Orkin C, DeJesus E, Khanlou H, Stoehr A, Supparatpinyo K, Lathouwers E, Lefebvre E, Opsomer M, Van de Casteele T, Tomaka F, Final 192-week efficacy and safety of once-daily darunavir/ritonavir compared with lopinavir/ritonavir in HIV-1-infected treatment-naïve patients in the ARTEMIS trial, HIV Med. 14 (2013) 49–59. doi:10.1111/j.1468-1293.2012.01060.x.

[8]. Louis JM, Aniana A, Weber IT, Sayer JM, Inhibition of autoprocessing of natural variants and multidrug resistant mutant precursors of HIV-1 protease by clinical inhibitors., Proc. Natl. Acad. Sci. U. S. A 108 (2011) 9072–7. doi:10.1073/pnas.1102278108. [PubMed: 21576495]

[9]. Huang L, Chen C, Autoprocessing of human immunodeficiency virus type 1 protease miniprecursor fusions in mammalian cells, AIDS Res. Ther 7 (2010) 27. doi:10.1186/1742-6405-7-27. [PubMed: 20667109]

[10]. Huang D, Caflisch A, How Does Darunavir Prevent HIV-1 Protease Dimerization?, J. Chem. Theory Comput 8 (2012) 1786–1794. doi:10.1021/ct300032r. [PubMed: 26593669]

[11]. Godfrey C, Thigpen MC, Crawford KW, Jean-Phillippe P, Pillay D, Persaud D, Kuritzkes DR, Wainberg M, Raizes E, Fitzgibbon J, Global HIV Antiretroviral Drug Resistance, J. Infect. Dis 216 (2017) S798–S800. doi:10.1093/infdis/jix137. [PubMed: 28973412]

[12]. Wensing AM, Calvez V, Günthard HF, Johnson VA, Paredes R, Pillay D, Shafer RW, Richman DD, 2017 Update of the Drug Resistance Mutations in HIV-1., Top. Antivir. Med 24 (2017) 132–133. http://www.ncbi.nlm.nih.gov/pubmed/28208121 (accessed November 29, 2018).

[13]. Weber IT, Kneller DW, Wong-Sam A, Highly resistant HIV-1 proteases and strategies for their inhibition, Future Med. Chem 7 (2015) 1023–1038. doi:10.4155/fmc.15.44. [PubMed: 26062399]

[14]. Agniswamy J, Louis JM, Roche J, Harrison RW, Weber IT, Structural Studies of a Rationally Selected Multi-Drug Resistant HIV-1 Protease Reveal Synergistic Effect of Distal Mutations on Flap Dynamics, PLoS One. 11 (2016) e0168616. doi:10.1371/journal.pone.0168616. [PubMed: 27992544]

[15]. Park JH, Sayer JM, Aniana A, Yu X, Weber IT, Harrison RW, Louis JM, Binding of Clinical Inhibitors to a Model Precursor of a Rationally Selected Multidrug Resistant HIV-1 Protease Is Significantly Weaker Than That to the Released Mature Enzyme, Biochemistry. 55 (2016) 2390–2400. doi:10.1021/acs.biochem.6b00012. [PubMed: 27039930]

[16]. Yedidi RS, Proteasa G, Martinez JL, Vickrey JF, Martin PD, Wawrzak Z, Liu Z, Kovari IA, Kovari LC, Contribution of the 80s loop of HIV-1 protease to the multidrug-resistance mechanism: crystallographic study of MDR769 HIV-1 protease variants., Acta Crystallogr. D. Biol. Crystallogr 67 (2011) 524–32. doi:10.1107/S0907444911011541. [PubMed: 21636892]

[17]. Kozísek M, Henke S, Sasková KG, Jacobs GB, Schuch A, Buchholz B, Müller V, Kräusslich H-GG, Rezácová P, Konvalinka J, Bodem J, Kožíšek M, Henke S, Šašková KG, Jacobs GB, Schuch A, Buchholz B, Müller V, Kräusslich H-GG, Řezáčová P, Konvalinka J, Bodem J, Mutations in HIV-1 gag and pol compensate for the loss of viral fitness caused by a highly mutated protease., Antimicrob. Agents Chemother 56 (2012) 4320–30. doi:10.1128/AAC.00465-12. [PubMed: 22644035]

[18]. Agniswamy J, Shen CH, Aniana A, Sayer JM, Louis JM, Weber IT, HIV-1 protease with 20 mutations exhibits extreme resistance to clinical inhibitors through coordinated structural rearrangements, Biochemistry. 51 (2012) 2819–2828. doi:10.1021/bi2018317. [PubMed: 22404139]

[19]. Dierynck I, De Wit M, Gustin E, Keuleers I, Vandersmissen J, Hallenberger S, Hertogs K, Binding Kinetics of Darunavir to Human Immunodeficiency Virus Type 1 Protease Explain the Potent Antiviral Activity and High Genetic Barrier, J. Virol 81 (2007) 13845–13851. doi:10.1128/JVI.01184-07. [PubMed: 17928344]

[20]. Shen C-H, Chang Y-C, Agniswamy J, Harrison RW, Weber IT, Conformational variation of an extreme drug resistant mutant of HIV protease., J. Mol. Graph. Model 62 (2015) 87–96. doi:10.1016/j.jmgm.2015.09.006. [PubMed: 26397743]

[21]. Ghosh AK, Martyr CD, Kassekert LA, Nyalapatla PR, Steffey M, Agniswamy J, Wang Y-FY-F, Weber IT, Amano M, Mitsuya H, Design, synthesis, biological evaluation and X-ray structural studies of HIV-1 protease inhibitors containing substituted fused-tetrahydropyranyl tetrahydrofuran as P2-ligands., Org. Biomol. Chem 13 (2015) 11607–21. doi:10.1039/c5ob01930c. [PubMed: 26462551]

[22]. Chetty S, Bhakat S, Martin AJM, Soliman MES, Multi-drug resistance profile of PR20 HIV-1 protease is attributed to distorted conformational and drug binding landscape: Molecular dynamics insights, J. Biomol. Struct. Dyn 34 (2016). doi:10.1080/07391102.2015.1018326.

[23]. Louis JM, Tözsér J, Roche J, Matúz K, Aniana A, Sayer JM, Enhanced Stability of Monomer Fold Correlates with Extreme Drug Resistance of HIV-1 Protease, Biochemistry. 52 (2013) 7678–7688. doi:10.1021/bi400962r. [PubMed: 24079831]

[24]. Agniswamy J, Shen C-H, Wang Y-F, Ghosh AK, Rao KV, Xu C-X, Sayer JM, Louis JM, Weber IT, Extreme multidrug resistant HIV-1 protease with 20 mutations is resistant to novel protease inhibitors with P1'-pyrrolidinone or P2-tris-tetrahydrofuran., J. Med. Chem 56 (2013) 4017–27. doi:10.1021/jm400231v. [PubMed: 23590295]

[25]. Agniswamy J, Louis JM, Shen C-H, Yashchuk S, Ghosh AK, Weber IT, Substituted *Bis*-THF Protease Inhibitors with Improved Potency against Highly Resistant Mature HIV-1 Protease

PR20., J. Med. Chem 58 (2015) 5088–95. doi:10.1021/acs.jmedchem.5b00474. [PubMed: 26010498]

[26]. Calcagno A, Di Perri G, Bonora S, Treating HIV Infection in the Central Nervous System, Drugs. 77 (2017) 145–157. doi:10.1007/s40265-016-0678-9. [PubMed: 28070871]

[27]. Ghosh AK, Rao KV, Nyalapatla PR, Kovela S, Brindisi M, Osswald HL, Sekhara Reddy B, Agniswamy J, Wang Y-F, Aoki M, Hattori S, Weber IT, Mitsuya H, Design of Highly Potent, Dual-Acting and Central-Nervous-System-Penetrating HIV-1 Protease Inhibitors with Excellent Potency against Multidrug-Resistant HIV-1 Variants, ChemMedChem. 13 (2018) 803–815. doi:10.1002/cmdc.201700824. [PubMed: 29437300]

[28]. Aoki M, Hayashi H, Rao KV, Das D, Higashi-Kuwata N, Bulut H, Aoki-Ogata H, Takamatsu Y, Yedidi RS, Davis DA, Hattori S, Nishida N, Hasegawa K, Takamune N, Nyalapatla PR, Osswald HL, Jono H, Saito H, Yarchoan R, Misumi S, Ghosh AK, Mitsuya H, A novel central nervous system-penetrating protease inhibitor overcomes human immunodeficiency virus 1 resistance with unprecedented aM to pM potency, Elife. 6 (2017) 1–25. doi:10.7554/eLife.28020.

[29]. Ghosh AK, Rao KV, Nyalapatla PR, Osswald HL, Martyr CD, Aoki M, Hayashi H, Agniswamy J, Wang Y-F, Bulut H, Das D, Weber IT, Mitsuya H, Design and Development of Highly Potent HIV-1 Protease Inhibitors with a Crown-Like Oxotricyclic Core as the P2-Ligand To Combat Multidrug-Resistant HIV Variants, J. Med. Chem (2017) acs.jmedchem.7b00172. doi:10.1021/acs.jmedchem.7b00172.

[30]. Hattori S-I, Hayashi H, Bulut H, Rao KV, Nyalapatla PR, Hasegawa K, Aoki M, Ghosh AK, Mitsuya H, Halogen bond interactions of novel HIV-1 protease inhibitors (PI)(GRL-001–15 and GRL-003–15) with the flap of protease are critical for their potent activity against wild-type and multi-PI-resistant HIV-1 variants., Antimicrob. Agents Chemother (2019) AAC.02635–18. doi:10.1128/AAC.02635-18.

[31]. Salcedo Gómez PM, Amano M, Yashchuk S, Mizuno A, Das D, Ghosh AK, Mitsuya H, GRL-04810 and GRL-05010, difluoride-containing nonpeptidic HIV-1 protease inhibitors (PIs) that inhibit the replication of multi-PI-resistant HIV-1 in vitro and possess favorable lipophilicity that may allow blood-brain barrier penetration., Antimicrob. Agents Chemother 57 (2013) 6110–21. doi:10.1128/AAC.01420-13. [PubMed: 24080647]

[32]. Ghosh AK, Yashchuk S, Mizuno A, Chakraborty N, Agniswamy J, Wang Y-F, Aoki M, Gomez PMS, Amano M, Weber IT, Mitsuya H, Design of gem -Difluoro- bis -Tetrahydrofuran as P2 Ligand for HIV-1 Protease Inhibitors to Improve Brain Penetration: Synthesis, X-ray Studies, and Biological Evaluation, ChemMedChem. 10 (2015) 107–115. doi:10.1002/cmdc.201402358. [PubMed: 25336073]

[33]. Agniswamy J, Kneller DW, Brothers R, Wang Y-F, Harrison RW, Weber IT, Highly Drug-Resistant HIV-1 Protease Mutant PRS17 Shows Enhanced Binding to Substrate Analogues, ACS Omega. 4 (2019) 8707–8719. doi:10.1021/acsomega.9b00683. [PubMed: 31172041]

[34]. Otwinowski Z, Minor W, Processing of X-ray diffraction data collected in oscillation mode, Elsevier, 1997. doi:10.1016/S0076-6879(97)76066-X.

[35]. McCoy AJ, Grosse-Kunstleve RW, Adams PD, Winn MD, Storoni LC, Read RJ, Phaser crystallographic software., J. Appl. Crystallogr 40 (2007) 658–674. doi:10.1107/S0021889807021206. [PubMed: 19461840]

[36]. Winn MD, Ballard CC, Cowtan KD, Dodson EJ, Emsley P, Evans PR, Keegan RM, Krissinel EB, Leslie AGW, McCoy A, McNicholas SJ, Murshudov GN, Pannu NS, Potterton EA, Powell HR, Read RJ, Vagin A, Wilson KS, Overview of the CCP4 suite and current developments., Acta Crystallogr. D. Biol. Crystallogr 67 (2011) 235–42. doi:10.1107/S0907444910045749. [PubMed: 21460441]

[37]. Emsley P, Cowtan K, Coot: model-building tools for molecular graphics., Acta Crystallogr. D. Biol. Crystallogr 60 (2004) 2126–32. doi:10.1107/S0907444904019158. [PubMed: 15572765]

[38]. Murshudov GN, Skubák P, Lebedev AA, Pannu NS, Steiner RA, Nicholls RA, Winn MD, Long F, Vagin AA, REFMAC5 for the refinement of macromolecular crystal structures., Acta Crystallogr. D. Biol. Crystallogr 67 (2011) 355–67. doi:10.1107/S0907444911001314. [PubMed: 21460454]

[39]. DeLano WL, Pymol: An open-source molecular graphics tool, CCP4 Newsl. Protein Crystallogr 40 (2002) 82–92.

[40]. King NM, Prabu-Jeyabalan M, Nalivaika EA, Wigerinck P, de Béthune M-P, Schiffer CA, Structural and thermodynamic basis for the binding of TMC114, a next-generation human immunodeficiency virus type 1 protease inhibitor., J. Virol 78 (2004) 12012–21. doi:10.1128/JVI.78.21.12012-12021.2004. [PubMed: 15479840]

[41]. Brower ET, Bacha UM, Kawasaki Y, Freire E, Inhibition of HIV-2 Protease by HIV-1 Protease Inhibitors in Clinical Use, Chem. Biol. Drug Des 71 (2008) 298–305. doi:10.1111/j.1747-0285.2008.00647.x. [PubMed: 18312292]

[42]. Flor-Parra F, Pérez-Pulido AJ, Pachón J, Pérez-Romero P, The HIV Type 1 Protease L10I Minor Mutation Decreases Replication Capacity and Confers Resistance to Protease Inhibitors, AIDS Res. Hum. Retroviruses 27 (2011) 65–70. doi:10.1089/aid.2010.0072. [PubMed: 21142921]

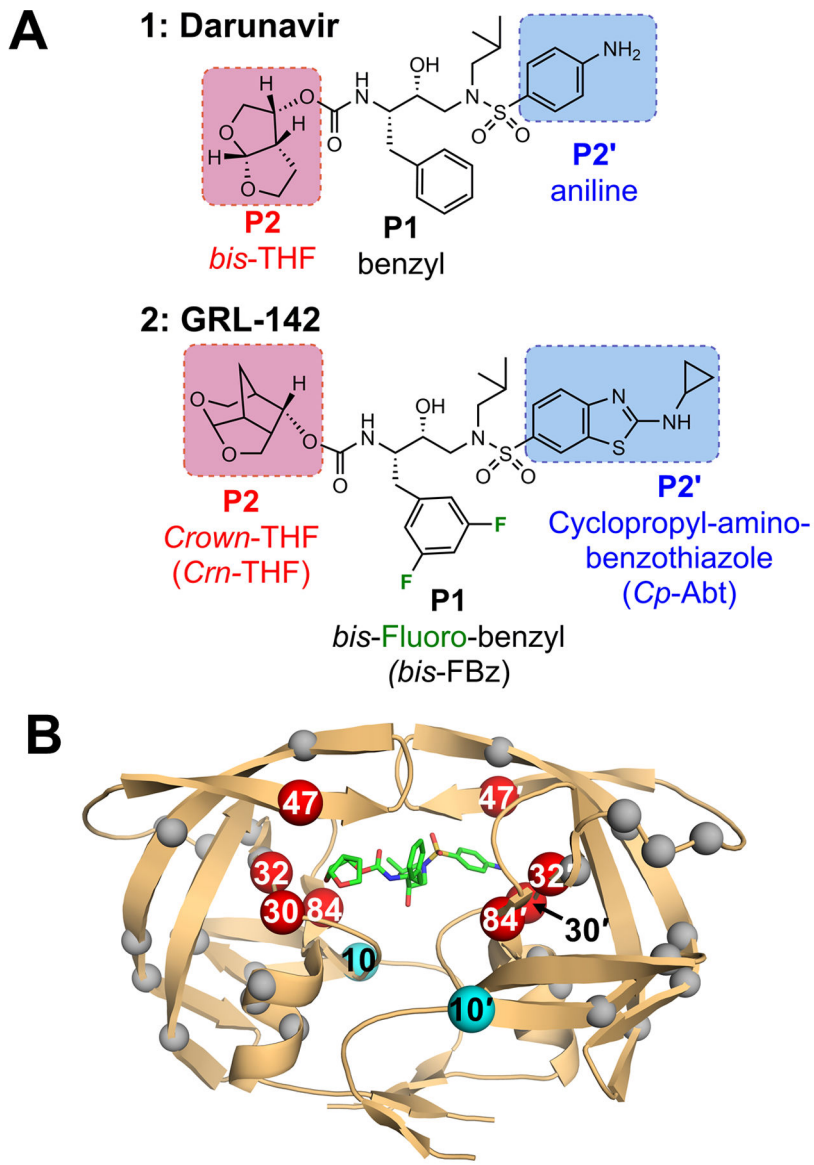

Figure 1: Chemical structures of compounds and PR20 dimer.

A. Inhibitor **1**: darunavir and Inhibitor **2**: GRL-142 differ at the P2, P2′, and P1 positions. B. Inhibitor **1** (green sticks) bound to the active site of the PR20 dimer (orange cartoon). PR20 contains 4 mutations in the inhibitor-binding site D30N, V32I, I47V, and I84V (red spheres). The L10F mutation (cyan spheres) sits near the dimer interface. Grey spheres indicate other mutations.

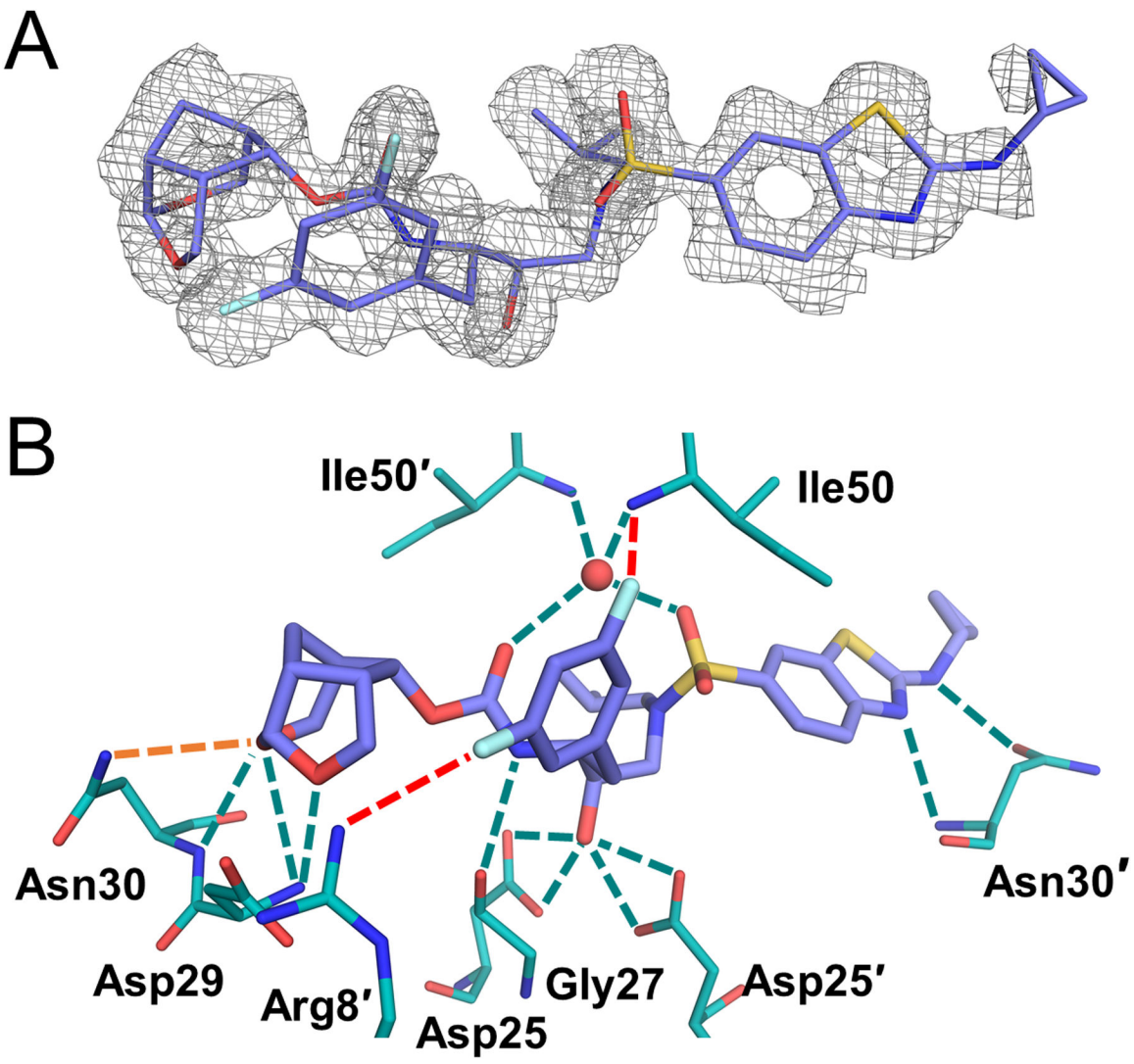

Figure 2. Inhibitor 2 bound in the active site of drug-resistant PR20.

A. Fo-Fc omit map (grey mesh) contoured at 2σ for the conformation of **2** (purple sticks) used for analysis. B. Polar interactions between **2** and PR20 residues (teal sticks). Dashed lines indicate hydrogen bonds (teal) and fluorine bonds (red dashes). New hydrogen bond in PR20/**2** is orange.

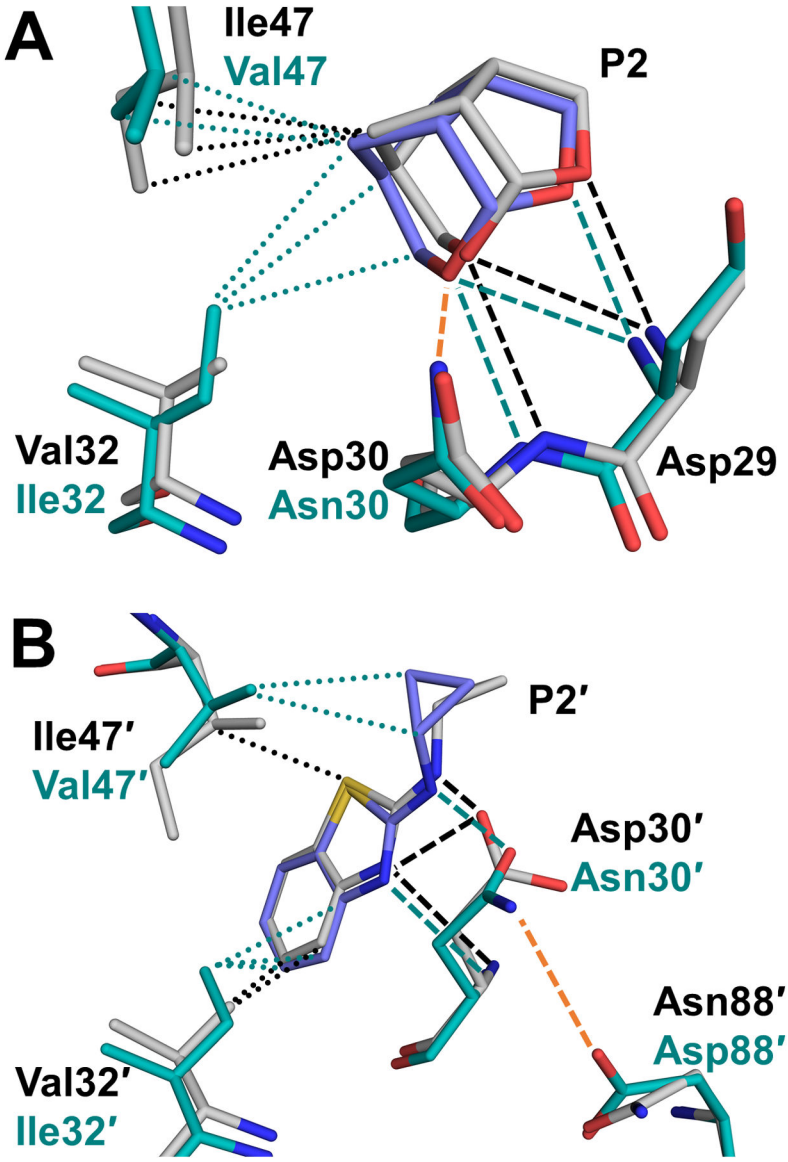

Figure 3: Interactions of the P2 and P2' groups of 2 in PR20/2 (purple/teal) compared to PR/2 (grey).

A. Comparison of P2 *Crn*-THF group interactions with residues in the S2 pocket of PR20 and PR. B. Comparison of P2′ Cp-Abt group interactions with residues in the S2′ pocket of PR20 and PR. Hydrogen bonds and van der Waals contacts are indicated as dashed and dotted lines, respectively, in teal for PR20/**2** and black for PR/**2**. Orange dashes indicate hydrogen bonds introduced in the PR20/**2** structure by mutations D30N and N88D.

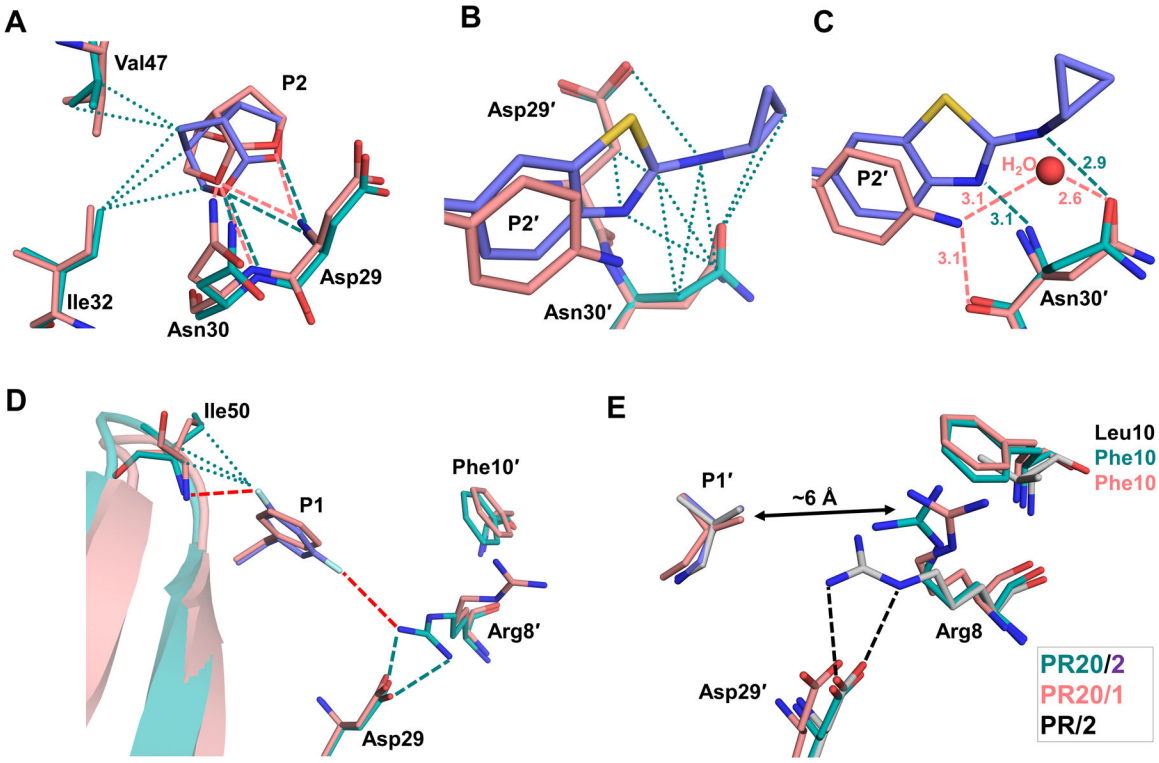

Figure 4. Comparison of interactions in PR20/1 (salmon) and PR20/2 (teal/purple).

A. Bulky P2 *Crn*-THF group of **2** creates 5 more van der Waals contacts with PR20 than does the *bis*-THF of **1**. B. Larger P2′ group on **2** adds van der Waals interactions with Asn30′ and Asp29′ side-chains that are absent in PR20/**1** structure. C. The P2′ Cp-Abt group of **2** forms direct hydrogen bonds with the mutated side-chain of D30′N, whereas the aniline group of **1** makes weaker water-mediated hydrogen bonds. Distances in Å. D. The *bis*-FBz of **2** makes fluoride bonds (red dashes) with Arg8′ and the tip of the flap at Ile50 that cannot be formed by the benzyl P1 of **1**. Intersubunit ion-pair between Arg8′ and Asp29 in PR20/**2** is lost in PR20/**1** since Arg8′ shifts toward mutated L10F. E. The short P1′-isobutyl in **1** and **2** cannot interact with Arg8 in PR20 or wild-type PR structures. Arg8 shifts toward mutated L10F in PR20 complexes instead of forming intersubunit ion pair observed in PR/**2** (grey).

Table 1:

Crystallographic Statistics

(Values in parentheses are for the highest resolution shell.)

	PR20/2
Resolution (Å)	50 – 1.21
Cell dimensions	
a (Å)	60.57
b (Å)	60.57
c (Å)	85.14
Space group	P 6_1
Unique Reflections	46,059
Completeness (%)	99.7 (89.8)
Redundancy	7.5 (2.3)
I/σ(I)	21.0 (2.0)
R_{merge} (%)	9.2 (44.8)
R_{work} (%)	15.2
R_{free} (%)	19.0
Solvent atoms	226
Average B-factors ($Å^2$)	
Protein	20.7
Inhibitor	13.8
Solvent	31.4
RMSD from ideality	
Bond lengths (Å)	0.015
Bond angles (°)	2.20